

Production of a Chiral Magnetic Anomaly with Emerging Turbulence and Mean-Field Dynamo Action

Jennifer Schober^{1,*}, Igor Rogachevskii^{2,3} and Axel Brandenburg^{3,4,5,6}

¹Laboratoire d'Astrophysique, EPFL, CH-1290 Sauverny, Switzerland

²Department of Mechanical Engineering, Ben-Gurion University of the Negev, P.O. Box 653, Beer-Sheva 84105, Israel

³Nordita, KTH Royal Institute of Technology and Stockholm University, 10691 Stockholm, Sweden

⁴Department of Astronomy, AlbaNova University Center, Stockholm University, 10691 Stockholm, Sweden

⁵School of Natural Sciences and Medicine, Ilia State University, 0194 Tbilisi, Georgia

⁶McWilliams Center for Cosmology and Department of Physics, Carnegie Mellon University, Pittsburgh, Pennsylvania 15213, USA

 (Received 27 July 2021; revised 12 November 2021; accepted 1 December 2021; published 9 February 2022)

In relativistic magnetized plasmas, asymmetry in the number densities of left- and right-handed fermions, i.e., a nonzero chiral chemical potential μ_5 , leads to an electric current along the magnetic field. This causes a chiral dynamo instability for a uniform μ_5 , but our simulations reveal a dynamo even for fluctuating μ_5 with zero mean. It produces magnetically dominated turbulence and generates mean magnetic fields via the magnetic α effect. Eventually, a universal scale-invariant k^{-1} spectrum of μ_5 and a k^{-3} magnetic spectrum are formed independently of the initial condition.

DOI: [10.1103/PhysRevLett.128.065002](https://doi.org/10.1103/PhysRevLett.128.065002)

The chiral magnetic effect (CME) is a macroscopic quantum phenomenon. It leads to an electric current along the magnetic field due to an imbalance between oppositely handed electrically charged fermions [1]. This is a direct consequence of the coupling of fermionic chirality and the topology of magnetic field lines characterized by magnetic helicity [2,3]. Chiral asymmetry is quantified by the chiral chemical potential $\mu_5 \equiv \mu_L - \mu_R$, which is nonzero in regions where the chemical potentials of left- (μ_L) and right-handed (μ_R) fermions differ. It has been shown [4] that μ_5 can survive down to energies of ≈ 10 MeV and thereby the CME can potentially affect leptogenesis during the QCD phase transition [5] and produce gravitational waves in the early Universe [6].

The dynamics of chiral fluids has been studied in various approaches [4,7–12], including an effective description called chiral magnetohydrodynamics (MHD) [13–16]. A significant difference to classical MHD is that the CME can induce a dynamo instability in the magnetic field on small length scales [17]. Unlike classical MHD dynamos, chiral dynamos can occur without an initial velocity field and self-consistently produce turbulence through the Lorentz force. This can activate a chiral mean-field dynamo [14,18–20].

The possibility of efficient magnetic field amplification through the CME has relevance for the early Universe. In particular, the transport of magnetic energy to large length scales via a chiral inverse cascade [4,21–23] and the chiral mean-field dynamo, strongly increases the chance of primordial magnetic fields [24,25] to survive until present day. Thereby, observational constraints on magnetic fields in cosmic voids [26] may open up a unique window into the fundamental physics of the early Universe. Beyond

cosmology, chiral MHD has also relevance to neutron stars [27–31], quark-gluon plasmas in heavy-ion collisions [2,3,32], and quantum materials [33].

In all previous chiral dynamo studies, a uniform initial μ_5 has been considered [14,18–20]. However, a uniform μ_5 requires special generation mechanisms. Therefore, we consider in this Letter a more general and universal situation with initial fluctuations of the chiral chemical potential, but zero mean.

For the analysis, we normalize μ_5 by $4\alpha_{\text{em}}/(\hbar c)$ such that it has the dimension of inverse length, where α_{em} is the fine structure constant, c is the speed of light, and \hbar is the reduced Planck constant. The strength of the coupling of the electromagnetic field to μ_5 is characterized by the chiral feedback parameter λ which, for hot plasmas, is given by $\lambda = 3\hbar c(8\alpha_{\text{em}})^2/(k_B T)^2$, where T is the temperature and k_B is the Boltzmann constant. We consider the following set of chiral MHD equations [14]:

$$\frac{\partial \mathbf{B}}{\partial t} = \nabla \times [\mathbf{U} \times \mathbf{B} - \eta(\nabla \times \mathbf{B} - \mu_5 \mathbf{B})], \quad (1)$$

$$\rho \frac{D\mathbf{U}}{Dt} = (\nabla \times \mathbf{B}) \times \mathbf{B} - \nabla p + \nabla \cdot (2\nu \rho \mathbf{S}), \quad (2)$$

$$\frac{D\rho}{Dt} = -\rho \nabla \cdot \mathbf{U}, \quad (3)$$

$$\frac{D\mu_5}{Dt} = \mathcal{D}_5(\mu_5) + \lambda \eta [\mathbf{B} \cdot (\nabla \times \mathbf{B}) - \mu_5 \mathbf{B}^2], \quad (4)$$

where the magnetic field \mathbf{B} is normalized such that the magnetic energy density is $\mathbf{B}^2/2$, and $D/Dt = \partial/\partial t + \mathbf{U} \cdot \nabla$

with \mathbf{U} being the velocity field. Further, η is the microscopic magnetic diffusivity, p is the fluid pressure, $\mathbf{S}_{ij} = (U_{i,j} + U_{j,i})/2 - \delta_{ij}(\nabla \cdot \mathbf{U})/3$ are the components of the trace-free strain tensor \mathbf{S} (commas denote partial spatial derivatives) and ν is the kinematic viscosity. We adopt an isothermal equation of state, $p = \rho c_s^2$, with c_s being the sound speed. Equations (1)–(4) imply that total chirality $\chi_{\text{tot}} \equiv \langle \mathcal{H} \rangle + 2\langle \mu_5 \rangle / \lambda$ is conserved, where angle brackets denote volume averaging. Here, $\langle \mathcal{H} \rangle \equiv \langle \mathbf{a} \cdot \mathbf{b} \rangle$ is the magnetic helicity with the vector potential \mathbf{A} and $\mathbf{B} = \nabla \times \mathbf{A}$.

At the initial time t_0 , we assume $\langle \mu_5 \rangle(t_0) = 0$, but nonzero fluctuations, μ_5' , i.e., $\langle \mu_5'^2 \rangle(t_0) \neq 0$. Initially, small fluctuations of \mathbf{B} with zero mean are present, while the velocity field vanishes. The fluctuations μ_5' result in an exponential growth of magnetic fluctuations due to the chiral dynamo. This instability is caused by the term $\nabla \times (v_5 \mathbf{B})$ in Eq. (1) with $v_5 = \eta \mu_5$ and has a growth rate $\gamma(k) = |v_5|k - \eta k^2$, with k being the wave number. This instability is referred to as the chiral dynamo [17] and occurs when $|v_5| > \eta k$. Its maximum growth rate is $\gamma_5 = v_5^2/4\eta$ and is attained at $k_5 = |\mu_5|/2$. We note that, while the $\nabla \times (v_5 \mathbf{B})$ term in Eq. (1) is formally similar to the kinetic α effect in classical mean-field MHD [14], the velocity v_5 is not produced by helical turbulence, but rather by the CME. During the chiral dynamo phase, magnetic fluctuations produce velocity fluctuations via the Lorentz force $(\nabla \times \mathbf{B}) \times \mathbf{B}$.

Since the initial mean chiral chemical potential is zero, and the initial small-scale magnetic helicity $\langle \mathbf{a} \cdot \mathbf{b} \rangle(t_0)$ related to the fluctuations of the vector potential \mathbf{a} and the magnetic field \mathbf{b} vanishes, we have $\chi_{\text{tot}}(t_0) = 0$. The initial μ_5' with a wide range of scales produces \mathbf{b} by the chiral dynamo. Indeed, for a wide spectrum in k space, fluctuations of μ_5 on larger scales serve as a *mean field* for fluctuations on smaller scales, so that the chiral dynamo instability excites \mathbf{b} and produces small-scale magnetic helicity $\langle \mathbf{a} \cdot \mathbf{b} \rangle$. Because of the conservation of total chirality, $\chi_{\text{tot}}(t) = 0$, the generation of $\langle \mathbf{a} \cdot \mathbf{b} \rangle$ causes growth of the mean chiral chemical potential, $\langle \mu_5 \rangle = -\lambda \langle \mathbf{a} \cdot \mathbf{b} \rangle / 2$. Simultaneously, the chiral dynamo drives turbulence magnetically and therefore enhances the fluid and magnetic Reynolds numbers, $\text{Re} \equiv U_{\text{rms}} / (\nu k_{\text{int}})$ and $\text{Re}_M \equiv U_{\text{rms}} / (\eta k_{\text{int}})$, where k_{int}^{-1} is the integral scale of magnetically driven turbulence. When Re_M is large enough, the mean-field dynamo instability is excited and amplifies a large-scale magnetic field. These theoretical ideas are now checked in DNS.

We use the PENCIL CODE [34] to solve Eqs. (1)–(4) with high-order finite difference methods in a 3D periodic domain of size $L^3 = (2\pi)^3$ with a resolution of 672^3 . The smallest wave number covered in the numerical domain is $k_1 = 2\pi/L = 1$ which we use for normalization of length scales. All velocities are normalized to $c_s = 1$ and the mean fluid density is $\bar{\rho} = 1$. Time is expressed in terms

of the resistive time $t_\eta = (\eta k_1^2)^{-1}$ with η being the microscopic diffusivity, which is a relevant constant throughout the DNS. We stress, however, that in magnetically driven turbulence, turbulent diffusion dominates shortly after the onset of the mean-field dynamo, yet it is not practical for normalization due to its time dependence.

For numerical stability, diffusion of μ_5 has to be applied in Eq. (4). To affect primarily the largest resolved wave numbers k in the simulation domain, we use hyperdiffusion, $\mathcal{D}_5(\mu_5) = -\mathcal{D}_5 \nabla^4 \mu_5$; see the companion paper [35] for technical details. In all runs, we use $\nu = \eta = 2 \times 10^{-4}$, i.e., $\text{Re}_M = \text{Re}$, which are based on the time-dependent integral scale of magnetically driven turbulence,

$$k_{\text{int}}^{-1} \equiv \frac{\int_1^{k_{\text{max}}} E_M(k) k^{-1} dk}{\int_1^{k_{\text{max}}} E_M(k) dk}. \quad (5)$$

Here, E_M is the magnetic energy spectrum, scaled such that $\int_0^{k_{\text{max}}} E_M(k, t) dk \equiv \langle \mathbf{B}^2 \rangle / 2$. Likewise, power spectra of μ_5 obey $\int_0^{k_{\text{max}}} E_5(k, t) dk \equiv \langle \mu_5'^2 \rangle$. As initial conditions we use $\mathbf{U} = \mathbf{0}$ and a weak seed magnetic field in form of Gaussian noise. Initial fluctuations of μ_5 are also set up as Gaussian noise, but with a specific spectrum that follows a power law in k space, i.e., $E_5(t_0) = E_{5,0}(k/k_1)^s \exp(-k^2/k_{\text{cut}}^2)$ with a cutoff k_{cut} that is needed for $s > -1$. We perform runs with $s = -2, -1, +1$ (see Table I) and the amplitude $E_{5,0}$ is chosen such that the maximum value of μ_5 in the domain is comparable for all runs at the time t_5 when the chiral dynamo starts. In all runs, the initial mean value of μ_5 is vanishing, so that $\chi_{\text{tot}} = \langle \mathcal{H} \rangle + 2\langle \mu_5 \rangle / \lambda \approx 0$, and we use $\lambda = 400$.

The fluctuations μ_5' result in an exponential growth of B_{rms} at the rate γ_5 due to the chiral dynamo, as can be seen in Fig. 1(a). Usage of $v_5 = \eta \mu_{5,\text{max}}$ in the expression for γ_5 with the maximum value of the chiral chemical potential, $\mu_{5,\text{max}}$, as shown in Fig. 1(b), reproduces the observed growth rate for all runs rather well; see Fig. 1(c) [and Fig. 3(b)]. We note, however, that a sufficient separation of scales is required for the dynamo to reach the maximum possible growth rate; see the accompanying paper [35]. When comparing the measured growth rate with γ_5 , we neglect the change of μ_5 in time, which is much smaller than the increase of B_{rms} . During the chiral dynamo phase, $\langle \mathcal{H} \rangle$ [Fig. 1(a)] and $\langle \mu_5 \rangle$ [Fig. 1(b)] are produced. If the divergence of magnetic helicity fluxes is small, the latter two always tend to have opposite signs, as follows from the

TABLE I. Summary of all runs.

Run	$E_5(k, t_0)$	$\mu_{5,\text{rms}}(t_0)$	$\mu_{5,\text{max}}(t_0)$	$\mu_{5,\text{max}}(t_5)$	$\max(\text{Re}_M)$
R - 2	$\propto k^{-2}$	13.8	50.5	48.1	288
R - 1	$\propto k^{-1}$	15.8	85.8	62.0	134
R + 1	$\propto k^1 e^{-(k/10)^2}$	12.6	53.7	53.7	65.1

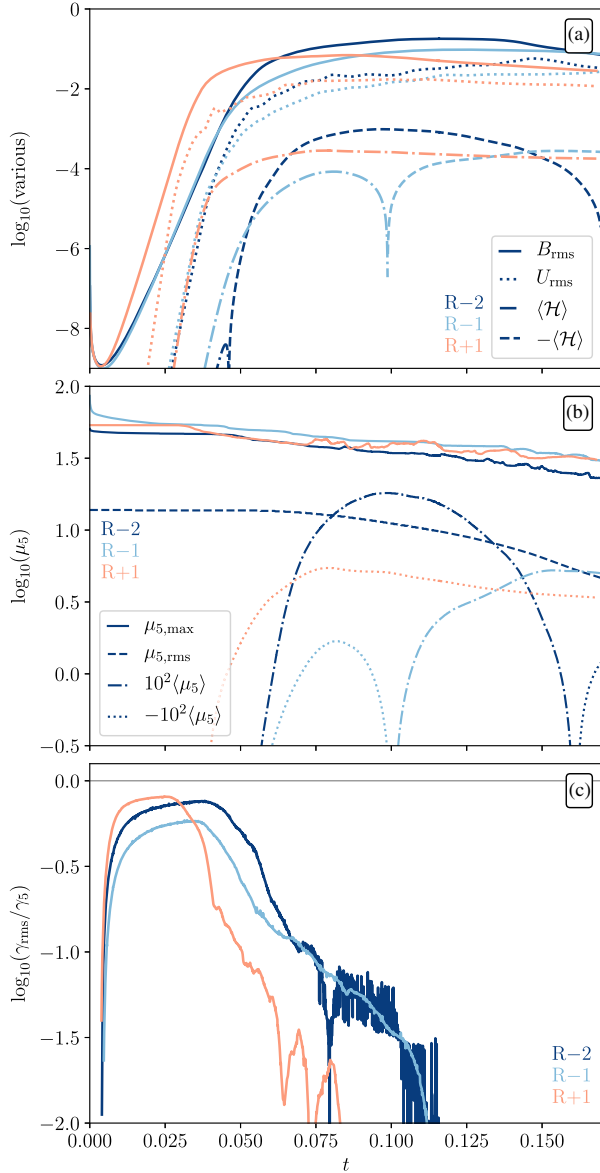


FIG. 1. Direct comparison between the time evolution of different quantities of all simulations. Different colors refer to different runs: R – 2 (dark blue), R – 1 (light blue), and R + 1 (orange). (a) Time series of B_{rms} , U_{rms} , and $\langle \mathcal{H} \rangle$. (b) Time series of $\mu_{5,\max}$ and $\langle \mu_5 \rangle$. The latter has been multiplied by a factor of 100 for better visualization. (c) Measured growth rate of B_{rms} , γ_{rms} , over $\gamma_5 = \eta \mu_{5,\max}^2 / 4$.

conservation of total chirality. Therefore, contrary to previously considered cases with an initially uniform μ_5 , the conservation law cannot be used to estimate the maximum magnetic field produced by the chiral dynamo. In the companion paper [35] we present a phenomenological model for the maximum magnetic field strength.

With magnetic field amplification via the chiral dynamo, velocity fluctuations are produced by the Lorentz force. When the turbulent velocity approaches the Alfvén speed, $U_{\text{rms}} \approx v_A \equiv B_{\text{rms}}$ (at $t \approx 0.03$ for run R + 1 and $t \approx 0.05$ for

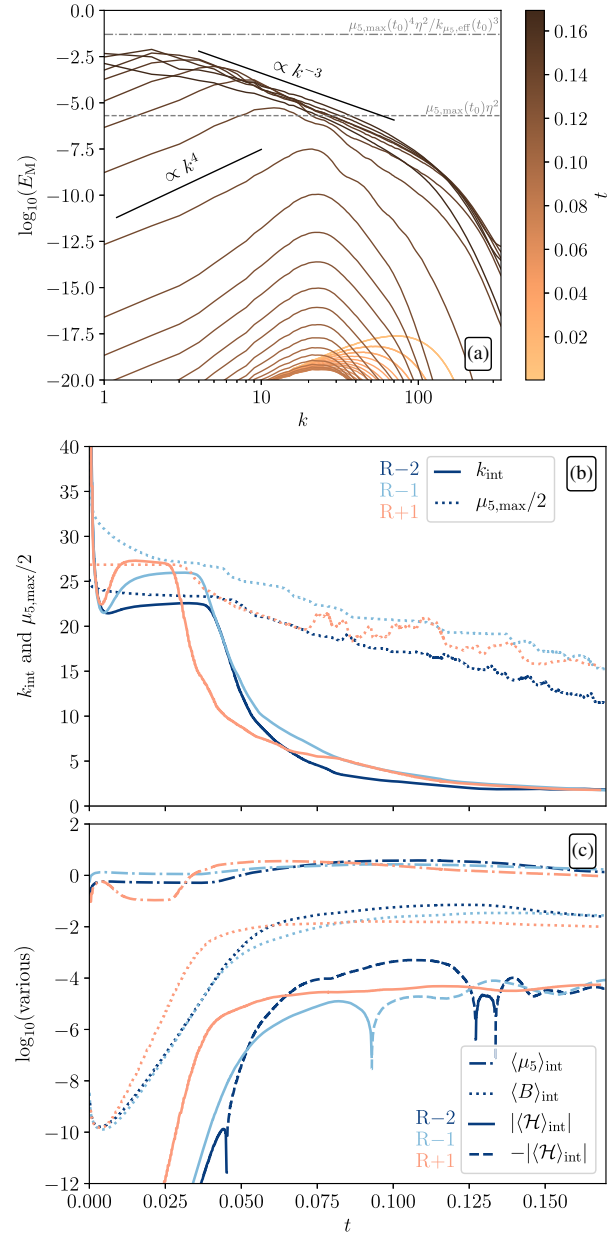


FIG. 2. (a) Time evolution of the magnetic energy spectrum E_M for run R – 2 with time indicated by the color bar. (b) The wave number based on the integral scale of turbulence, k_{int} , as a function of time for all runs (solid lines) and the value of the theoretically predicted wave number, $\mu_{5,\max}/2$, on which the v_5 dynamo instability has the largest growth rate (dotted lines). (c) Different averages based on the k_{int} : $\langle \mu_5 \rangle_{\text{int}}$ (dashed-dotted), $\langle B \rangle_{\text{int}}$ (dotted lines), $\langle \mathcal{H} \rangle_{\text{int}}$ (solid lines), and $-\langle \mathcal{H} \rangle_{\text{int}}$ (dashed lines).

runs R – 2 and R – 1) the small-scale chiral dynamo phase ends. This coincides with the time t_{IC} when the peak of the magnetic energy spectrum reaches $\eta^2 \mu_{5,\max}(t_0)$ and starts to shift to larger scales; see E_M for run R – 2 in Fig. 2(a).

In such chiral-magnetically driven turbulence, a mean-field dynamo instability can occur if Re and Re_M are large. To study the mean-field dynamo, we perform averages

$\langle \mu_5 \rangle_{\text{int}}$, $\langle \mathcal{B} \rangle_{\text{int}}$, and $\langle \mathcal{H} \rangle_{\text{int}}$ on the scale k_{int} [see Fig. 2(b)], defined as

$$\langle X \rangle_{\text{int}} = \left[\frac{\int_0^{k_{\text{max}}} E_M(k) E_X(k) dk}{\int_0^{k_{\text{max}}} E_M(k) dk} \right]^{1/2}, \quad (6)$$

where $E_X(k)$ is the spectrum of X ; see Fig. 2(c).

The mean-field dynamo instability has a maximum growth rate of $\gamma_\alpha = (\eta \langle \mu_5 \rangle_{\text{int}} + \alpha_\mu + \alpha_M + \alpha_K)^2 / (4\eta_T)$, where $\eta_T \approx U_{\text{rms}} / (3k_{\text{int}})$ is the turbulent magnetic diffusivity. The different α effects are approximately given by $\alpha_\mu = -(2/3)\eta \langle \mu_5 \rangle_{\text{int}} \log(\text{Re}_M)$ [14], the magnetic α effect, $\alpha_M = 2(q-1)/(q+1)\tau_c \chi_c$, and the kinetic α effect, $\alpha_K = -(1/3)\tau_c \chi_K$. Here, $\chi_c = \langle \mathbf{b} \cdot (\nabla \times \mathbf{b}) \rangle_{\text{int}} \approx \langle \mathbf{a} \cdot \mathbf{b} \rangle_{\text{int}} k_{\text{int}}^2$ is the current helicity, $\chi_K = \langle \mathbf{u} \cdot \boldsymbol{\omega} \rangle_{\text{int}}$ is the kinetic helicity, $\boldsymbol{\omega} \equiv \nabla \times \mathbf{u}$ is the vorticity, $\tau_c \approx (v_A k_{\text{int}})^{-1}$ is the correlation time of magnetically driven turbulence, and q is the slope of the magnetic energy spectrum $\propto k^{-q}$. We use $q = 3$; see Fig. 2(a). Figure 3(a) shows that α_M dominates once turbulence is produced and therefore the mean-field dynamo growth rate is $\gamma_\alpha \approx \alpha_M^2 / (4\eta_T)$.

Our DNS indicate that χ_c plays the key role for the mean-field dynamo sourced by initially inhomogeneous fluctuations of μ_5 ; see Fig. 3(a) and the accompanying paper [35]. The evolution of χ_c is closely connected to that of the small-scale magnetic helicity [14]:

$$\frac{\partial}{\partial t} \overline{\mathbf{a} \cdot \mathbf{b}} + \text{div} \mathbf{F} = 2\bar{v}_5 \bar{\mathbf{b}}^2 - 2\bar{\boldsymbol{\mathcal{E}}} \cdot \bar{\mathbf{B}} - 2\eta \bar{\mathbf{b}} \cdot (\nabla \times \bar{\mathbf{b}}), \quad (7)$$

where $\bar{\boldsymbol{\mathcal{E}}} \equiv \overline{\mathbf{u} \times \mathbf{b}} = \alpha_M \bar{\mathbf{B}} - \eta_T (\nabla \times \bar{\mathbf{B}})$ is the electromotive force with α_M being the dominant contribution to the total α effect, and \mathbf{F} is the flux of $\overline{\mathbf{a} \cdot \mathbf{b}}$. Near magnetic field maximum, two leading source or sink terms in Eq. (7), $2\bar{v}_5 \bar{\mathbf{b}}^2 - 2\alpha_M \bar{\mathbf{B}}^2$, compensate each other, so that the magnetic α effect reaches the value $\alpha_M^{\text{sat}} = \eta \bar{\mu}_5 \bar{\mathbf{b}}^2 / \bar{\mathbf{B}}^2$. For $R = 2$, $|\alpha_M| \approx |\alpha_M^{\text{sat}}|$ for $t \gtrsim 0.075$, as can be seen in Fig. 3(a).

The maximum growth rate of the mean-field dynamo instability γ_α agrees well with the measured growth rate γ_{int} of $\langle \mathcal{B} \rangle_{\text{int}}$; see Fig. 3(b) for run R-2 in the interval $0.075 < t < 0.12$. In our DNS, γ_{int} strongly decreases when the scale at which γ_α is maximum becomes larger than the size of the box. As can be seen in Fig. 3(b), γ_{int}

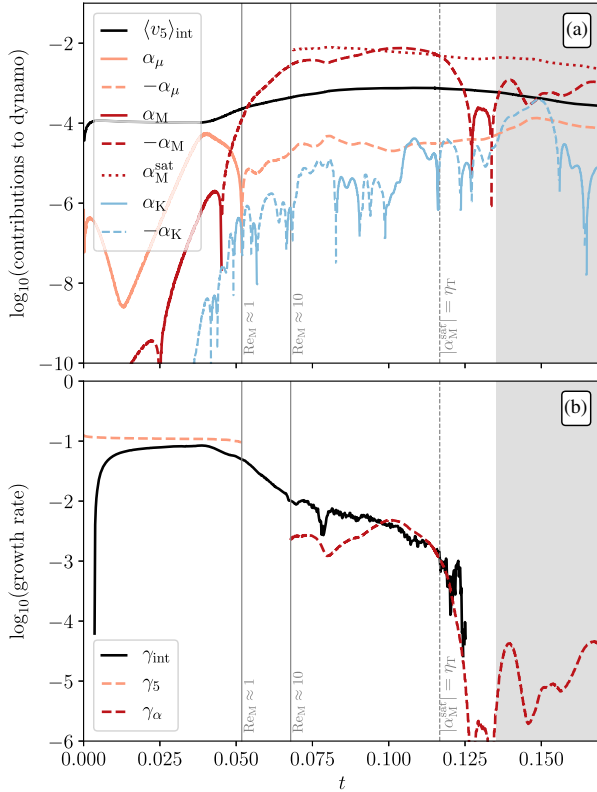


FIG. 3. Time evolution of different quantities in Run R-2. Gray background indicates that the inverse cascade has reached the size of the domain. (a) Different contributions to the mean-field dynamo growth rate, including $\langle v_5 \rangle_{\text{int}} \equiv \eta \langle \mu_5 \rangle_{\text{int}}$. (b) The measured growth rate of $\langle \mathcal{B} \rangle_{\text{int}}$, γ_{int} (black solid line) compared to the chiral dynamo growth rate γ_5 (orange dashed line), and the mean-field dynamo growth rate γ_α based on α_M (red dashed line).

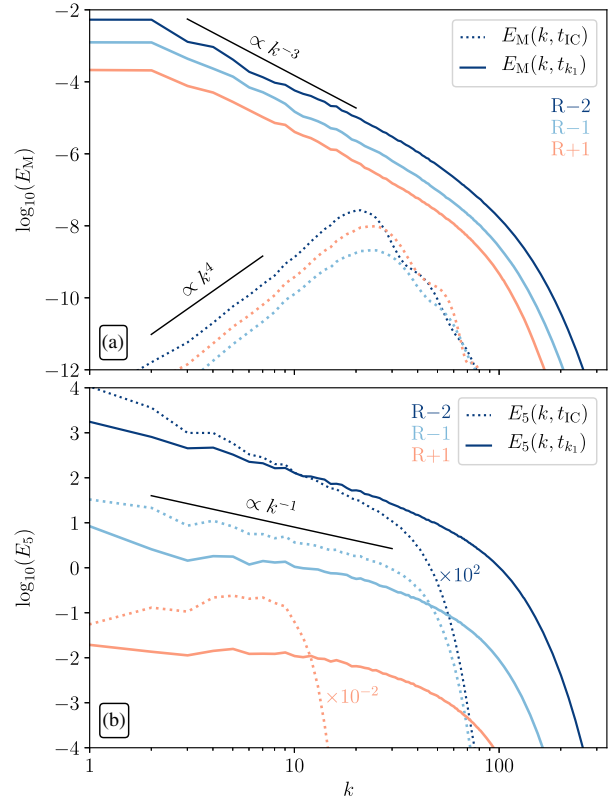


FIG. 4. Power spectra from all simulations. (a) Magnetic energy spectra E_M at the beginning of the chiral inverse cascade t_{IC} (dotted lines) and the time when the cascade reaches the size of the numerical domain t_{k_1} (solid lines). (b) Spectra of μ_5 shown at the same two characteristic times as E_M . For better visibility the spectra of runs R-2 and R+1 have been multiplied by factors of 10^2 and 10^{-2} , respectively.

vanishes once the positive contribution to the growth rate on the minimum wave number of the box, $|\alpha_M^{\text{sat}}|k_1$, becomes comparable to the negative contribution, $\eta_T k_1^2$. For $R - 2$, dissipation due to $\eta_T k_1^2$ on the box scale dominates for $t \gtrsim 0.12$.

At the time t_{k_1} when the peak of the magnetic energy reaches the size of the domain, all of the μ_5 spectra approach a universal k^{-1} ; see Fig. 4. The magnetic energy spectra approach a k^{-3} scaling which is, for fully helical magnetic fields, consistent with the magnetic helicity spectra $\propto k^{-4}$.

In conclusion, a small-scale chiral dynamo can arise from an initially fluctuating chiral chemical potential with zero mean. The chiral dynamo generates small-scale magnetic helicity which (i) produces a mean μ_5 due to the conservation of total chirality and (ii) drives turbulence via the Lorentz force. In our DNS, sufficiently strong turbulence is generated to activate a mean-field dynamo that is well described by the magnetic α effect caused by current helicity. During the mean-field dynamo phase, the power spectra develop a universal shape; $E_M \propto k^{-3}$ and $E_5 \propto k^{-1}$. In particular, with the onset of turbulence in the system, μ_5 becomes scale invariant, independent of its initial condition.

We have benefited from stimulating discussions with Abhijit B. Bendre, Nathan Kleeorin, and Matthias Rheinhardt. J. S. acknowledges the support by the Swiss National Science Foundation under Grant No. 185863. A. B. was supported in part through a grant from the Swedish Research Council (Vetenskapsrådet, 2019-04234).

*jennifer.schober@epfl.ch

- [1] A. Vilenkin, Equilibrium parity violating current in a magnetic field, *Phys. Rev. D* **22**, 3080 (1980).
- [2] D. E. Kharzeev, The chiral magnetic effect and anomaly-induced transport, *Prog. Part. Nucl. Phys.* **75**, 133 (2014).
- [3] D. E. Kharzeev, J. Liao, S. A. Voloshin, and G. Wang, Chiral magnetic and vortical effects in high-energy nuclear collisions-A status report, *Prog. Part. Nucl. Phys.* **88**, 1 (2016).
- [4] A. Boyarsky, J. Fröhlich, and O. Ruchayskiy, Self-Consistent Evolution of Magnetic Fields and Chiral Asymmetry in the Early Universe, *Phys. Rev. Lett.* **108**, 031301 (2012).
- [5] D. J. Schwarz and M. Stuke, Lepton asymmetry and the cosmic QCD transition, *J. Cosmol. Astropart. Phys.* **11** (2009) 025.
- [6] A. Brandenburg, Y. He, T. Kahniashvili, M. Rheinhardt, and J. Schober, Relic gravitational waves from the chiral magnetic effect, *Astrophys. J.* **911**, 110 (2021).
- [7] D. G. Figueroa, A. Florio, and M. Shaposhnikov, Chiral charge dynamics in Abelian gauge theories at finite temperature, *J. High Energy Phys.* **10** (2019) 142.
- [8] M. Mace, N. Mueller, S. Schlichting, and S. Sharma, Chiral Instabilities and the Onset of Chiral Turbulence in QED Plasmas, *Phys. Rev. Lett.* **124**, 191604 (2020).
- [9] M. A. Stephanov and Y. Yin, Chiral Kinetic Theory, *Phys. Rev. Lett.* **109**, 162001 (2012).
- [10] J.-Y. Chen, D. T. Son, and M. A. Stephanov, Collisions in Chiral Kinetic Theory, *Phys. Rev. Lett.* **115**, 021601 (2015).
- [11] E. V. Gorbar, I. A. Shovkovy, S. Vilchinskii, I. Rudenok, A. Boyarsky, and O. Ruchayskiy, Anomalous Maxwell equations for inhomogeneous chiral plasma, *Phys. Rev. D* **93**, 105028 (2016).
- [12] N. Yamamoto and D.-L. Yang, Chiral radiation transport theory of neutrinos, *Astrophys. J.* **895**, 56 (2020).
- [13] M. Giovannini, Anomalous magnetohydrodynamics, *Phys. Rev. D* **88**, 063536 (2013).
- [14] I. Rogachevskii, O. Ruchayskiy, A. Boyarsky, J. Fröhlich, N. Kleeorin, A. Brandenburg, and J. Schober, Laminar and turbulent dynamos in chiral magnetohydrodynamics I: Theory, *Astrophys. J.* **846**, 153 (2017).
- [15] L. Del Zanna and N. Bucciantini, Covariant and 3 + 1 equations for dynamo-chiral general relativistic magnetohydrodynamics, *Mon. Not. R. Astron. Soc.* **479**, 657 (2018).
- [16] K. Hattori, Y. Hirono, H.-U. Yee, and Y. Yin, Magnetohydrodynamics with chiral anomaly: Phases of collective excitations and instabilities, *Phys. Rev. D* **100**, 065023 (2019).
- [17] M. Joyce and M. Shaposhnikov, Primordial Magnetic Fields, Right Electrons, and the Abelian Anomaly, *Phys. Rev. Lett.* **79**, 1193 (1997).
- [18] J. Schober, I. Rogachevskii, A. Brandenburg, A. Boyarsky, J. Fröhlich, O. Ruchayskiy, and N. Kleeorin, Laminar and turbulent dynamos in chiral magnetohydrodynamics II. Simulations, *Astrophys. J.* **858**, 124 (2018).
- [19] J. Schober, A. Brandenburg, I. Rogachevskii, and N. Kleeorin, Energetics of turbulence generated by chiral MHD dynamos, *Geophys. Astrophys. Fluid Dyn.* **113**, 107 (2019).
- [20] J. Schober, A. Brandenburg, and I. Rogachevskii, Chiral fermion asymmetry in high-energy plasma simulations, *Geophys. Astrophys. Fluid Dyn.* **114**, 106 (2020).
- [21] Y. Hirono, D. E. Kharzeev, and Y. Yin, Self-similar inverse cascade of magnetic helicity driven by the chiral anomaly, *Phys. Rev. D* **92**, 125031 (2015).
- [22] E. V. Gorbar, I. Rudenok, I. A. Shovkovy, and S. Vilchinskii, Anomaly-driven inverse cascade and inhomogeneities in a magnetized chiral plasma in the early universe, *Phys. Rev. D* **94**, 103528 (2016).
- [23] A. Brandenburg, J. Schober, I. Rogachevskii, T. Kahniashvili, A. Boyarsky, J. Fröhlich, O. Ruchayskiy, and N. Kleeorin, The turbulent chiral-magnetic cascade in the early universe, *Astrophys. J. Lett.* **845**, L21 (2017).
- [24] K. Subramanian, The origin, evolution and signatures of primordial magnetic fields, *Rep. Prog. Phys.* **79**, 076901 (2016).
- [25] T. Vachaspati, Progress on cosmological magnetic fields, *Rep. Prog. Phys.* **84**, 074901 (2021).
- [26] A. Neronov and I. Vovk, Evidence for strong extragalactic magnetic fields from Fermi observations of TeV blazars, *Science* **328**, 73 (2010).
- [27] M. Dvornikov and V. B. Semikoz, Magnetic helicity evolution in a neutron star accounting for the Adler-Bell-Jackiw anomaly, *J. Cosmol. Astropart. Phys.* **08** (2018) 021.
- [28] Y. Masada, K. Kotake, T. Takiwaki, and N. Yamamoto, Chiral magnetohydrodynamic turbulence in core-collapse supernovae, *Phys. Rev. D* **98**, 083018 (2018).

- [29] N. Yamamoto, Chiral transport of neutrinos in supernovae: Neutrino-induced fluid helicity and helical plasma instability, *Phys. Rev. D* **93**, 065017 (2016).
- [30] G. Sigl and N. Leite, Chiral magnetic effect in protoneutron stars and magnetic field spectral evolution, *J. Cosmol. Astropart. Phys.* **01** (2016) 025.
- [31] M. Dvornikov, V. B. Semikoz, and D. D. Sokoloff, Generation of strong magnetic fields in a nascent neutron star accounting for the chiral magnetic effect, *Phys. Rev. D* **101**, 083009 (2020).
- [32] Y. Hirono, D. E. Kharzeev, and Y. Yin, New quantum effects in relativistic magnetohydrodynamics, *Nucl. Phys.* **A967**, 840 (2017).
- [33] V. Galitski, M. Kargarian, and S. Syzranov, Dynamo effect and turbulence in hydrodynamic Weyl metals, *Phys. Rev. Lett.* **121**, 176603 (2018).
- [34] A. Brandenburg *et al.* (Pencil Code Collaboration), The Pencil Code, a modular MPI code for partial differential equations and particles: Multipurpose and multiuser-maintained, *J. Open Source Software* **6**, 2807 (2021).
- [35] J. Schober, I. Rogachevskii, and A. Brandenburg, companion paper, Dynamo instabilities in plasmas with inhomogeneous chiral chemical potential, *Phys. Rev. D* **105**, 043507 (2022).